

Second-harmonic generation and linear electro-optical coefficients of BN nanotubes

G.Y. Guo* and J.C. Lin

*Department of Physics, National Taiwan University,
Taipei, Taiwan 106, Republic of China*

(Dated: October 24, 2018)

Abstract

A systematic *ab initio* study of the second-order nonlinear optical properties of BN nanotubes within density functional theory in the local density approximation has been performed. Highly accurate full-potential projector augmented-wave method was used. Specifically, the second-harmonic generation ($\chi_{abc}^{(2)}$) and linear electro-optical (r_{abc}) coefficients of a large number of the single-walled zigzag, armchair and chiral BN nanotubes (BN-NT) as well as the double-walled zigzag (12,0)@(20,0) BN nanotube and the single-walled zigzag (12,0) BN-NT bundle have been calculated. Importantly, unlike carbon nanotubes, both the zigzag and chiral BN-NTs are found to exhibit large second-order nonlinear optical behavior with the $\chi_{abc}^{(2)}$ and r_{abc} coefficients being up to thirty times larger than that of bulk BN in both zinc-blende and wurtzite structures, indicating that BN-NTs are promising materials for nonlinear optical and opto-electric applications. Though the interwall interaction in the double-walled BN-NTs is found to reduce the second-order nonlinear optical coefficients significantly, the interwall interaction in the single-walled BN-NT bundle has essentially no effect on the nonlinear optical properties. The prominent features in the spectra of $\chi_{abc}^{(2)}(-2\omega, \omega, \omega)$ of the BN-NTs are successfully correlated with the features in the linear optical dielectric function $\varepsilon(\omega)$ in terms of single-photon and two-photon resonances.

PACS numbers: 78.67.Ch, 42.65.Ky, 42.70.Mp

* Electronic address: gyguo@phys.ntu.edu.tw

I. INTRODUCTION

Since their discovery in 1991¹, carbon nanotubes (CNTs) have attracted considerable interest worldwide because of their unusual properties and great potentials for technological applications. For example, because of their one-dimensional character, metallic CNTs are quantum wires that may exhibit exotic Luttinger-liquid behavior rather than usual Fermi-liquid behavior in normal metal wires.² It was also predicted that nanotori formed from metallic CNTs may exhibit giant paramagnetic moments.³ Furthermore, chiral CNTs are expected to exhibit a number of unusual optical properties such as optical activity, circular dichroism and second harmonic generation (see ^{4,5} and references therein).

Soon after the discovery of CNTs it became obvious that similar nanostructures could be formed by other elements and compounds which form layered structures bearing some resemblance to graphite. For example, hexagonal BN (*h*-BN) was predicted on the basis of theoretical calculations^{6,7} to be capable of forming nanotubes, a prediction which was later confirmed experimentally by the synthesis of such nanotubes.⁸ Both single-walled and multi-walled BN nanotubes (BN-NT) can now be readily synthesized.⁹ Though CNTs continue to attract great interest, other nanotubes such as BN-NTs are interesting in their own right and may be able to offer different possibilities for technological applications that CNTs cannot provide. In particular, as far as the optical and opto-electronic applications of nanotubes are concerned, BN-NT could be superior to CNTs because BN-NTs are uniformly insulating, independent of their chirality. Furthermore, BN-NTs tend to have a zigzag structure.⁹ Though it is interesting that, depending on their chirality, CNTs can be metallic or semi-conducting or insulating⁴, it is still impossible to grow CNTs with a pre-specified chirality at present. Finally, recent experiments indicate that BN-NTs exhibit stronger resistance to oxidation at high temperatures than CNTs¹⁰

Therefore, the electronic, optical and other properties of both single-walled and multi-walled BN-NTs are interesting and have been intensively studied theoretically in recent years (see, e.g., ^{6,7,11,12,13,14,15,16,17,18}). In particular, Chen *et al.*¹⁵ calculated the transverse dielectric function of bundles of single-walled BN-NTs using a tight-binding model. Ng and Zhang¹⁸ calculated the optical absorption spectra of single-walled BN-NTs within a time-dependent localized-density-matrix approach based on a semiempirical Hamiltonian. Despite of these intensive theoretical studies, only few *ab initio* calculations of the optical

properties of BN-NTs have been reported¹⁹ because of the heavy demand of the computing resources. Semiempirical tight-binding model is known to describe well only the electronic excitations near the band gap of the large radius BN-NTs. Systematic *ab initio* calculations of the optical properties are thus needed in order to quantitatively interpret the optical experiments and to predict the BN-NTs with desired optical properties. Therefore, we have recently carried out a series of *ab initio* calculations²⁰ in order to analyze the band structure and linear optical features of all the three types of the BN-NTs and their possible dependence on diameter and chirality. In this work, we investigate the second-order optical susceptibility and also linear electro-optical coefficient of the BN-NTs. The primary objective is to find out the features and magnitude of the second-harmonic generation and linear electro-optical coefficients of the BN-NTs in order to see whether they have any potential applications in nonlinear optical and electro-optical devices such as second-harmonic generation, sum-frequency generation and electrical optical switch. The second objective is to identify characteristic differences in nonlinear optical properties between BN-NTs and CNTs.

The rest of this paper is organized as follows. In Sec. II, the theoretical approach and computational details are briefly described. In Sec. III, the calculated second-order nonlinear optical susceptibility and linear electro-optical coefficients of *h*-BN, single hexagonal BN sheet, and BN nanotubes are presented and analyzed. Finally, in Sec. IV, a summary is given.

II. THEORY AND COMPUTATIONAL METHOD

BN-NTs can be considered as a layer of graphitic BN sheet rolled up into a cylinder, and the structure of a BN-NT is completely specified by the chiral vector which is given in term of a pair of integers (n,m) .^{6,21} As for CNTs, BN-NTs are classified into three types, namely, armchair (n,n) nanotubes, zigzag $(n,0)$ nanotubes, and chiral (n,m) nanotubes with $n \neq m$.^{6,21} We consider a large number of representative BN-NTs with a range of diameters from all three types, namely, the zigzag $[(n,0), n = 5, 6, 8, 9, 12, 13, 15, 16, 17, 20, 21, 24, 25, 27]$, armchair $[(n,n), n = 4, 5, 6, 8, 12, 15]$, and chiral $(4,2), (6,4), (8,4), (10,5)$ BN-NTs. The double-walled zigzag $(12,0)@(20,0)$ BN nanotube and the single-walled zigzag $(12,0)$ BN-NT bundle have also been investigated to see the effects of interwall interaction. Our

ab initio calculations for the BN-NTs were performed using highly accurate full-potential projector augmented-wave (PAW) method²², as implemented in the VASP package²³. They are based on density functional theory (DFT) with the local density approximation (LDA). A supercell geometry was adopted so that the nanotubes are aligned in a square array with the closest distance between adjacent nanotubes being at least 6 Å. A large plane-wave cut-off of 450 eV was used throughout.

Firstly, the ideal nanotubes were constructed by rolling-up a hexagonal BN sheet. Their atomic positions and lattice constants were then fully relaxed by a conjugate gradient technique. Theoretical equilibrium nanotube structures were obtained when the forces acting on all the atoms and the uniaxial stress were less than 0.03 eV/Å and 2.0 kBar, respectively. The theoretical equilibrium lattice constants T and curvature energies E_c (total energy relative to that of single BN sheet) as well as the computational details have been reported before²⁰.

The self-consistent electronic band structure calculations were then carried out for the theoretically determined BN-NT structures. In this work, the non-linear optical properties were calculated based on the independent-particle approximation, i.e., the excitonic effects and the local-field corrections were neglected. As reported before²⁰, the dielectric function of *h*-BN calculated within the single-electron picture are in reasonably good agreement with experiments. Therefore, it might be expected that the independent-particle approximation could work rather well for the non-linear optical properties of the BN-NTs too. Following previous nonlinear optical calculations^{4,24}, the imaginary part of the second-order optical susceptibility due to direction interband transitions is given by²⁵

$$\chi_{abc}^{''(2)}(-2\omega, \omega, \omega) = \chi_{abc,VE}^{''(2)}(-2\omega, \omega, \omega) + \chi_{abc,VH}^{''(2)}(-2\omega, \omega, \omega) \quad (1)$$

where the contribution due to the so-called virtual-electron (VE) process is

$$\begin{aligned} \chi_{abc,VE}^{''(2)} = & -\frac{\pi}{2\Omega} \sum_{i \in VB} \sum_{j,l \in CB} \sum_{\mathbf{k}} w_{\mathbf{k}} \left\{ \frac{Im[p_{jl}^a \langle p_{li}^b p_{ij}^c \rangle]}{\epsilon_{li}^3(\epsilon_{li} + \epsilon_{ji})} \delta(\epsilon_{li} - \omega) \right. \\ & \left. - \frac{Im[p_{ij}^a \langle p_{jl}^b p_{li}^c \rangle]}{\epsilon_{li}^3(2\epsilon_{li} - \epsilon_{ji})} \delta(\epsilon_{li} - \omega) + \frac{16Im[p_{ij}^a \langle p_{jl}^b p_{li}^c \rangle]}{\epsilon_{ji}^3(2\epsilon_{li}^3 - \epsilon_{ji}^3)} \delta(\epsilon_{ji} - 2\omega) \right\} \end{aligned} \quad (2)$$

and that due to the virtual-hole (VH) process

$$\begin{aligned} \chi_{abc,VH}^{(2)} = & \frac{\pi}{2\Omega} \sum_{i,l \in VB} \sum_{j \in CB} \sum_{\mathbf{k}} w_{\mathbf{k}} \left\{ \frac{Im[p_{li}^a \langle p_{ij}^b p_{jl}^c \rangle]}{\epsilon_{jl}^3(\epsilon_{jl} + \epsilon_{ji})} \delta(\epsilon_{jl} - \omega) \right. \\ & \left. - \frac{Im[p_{ij}^a \langle p_{jl}^b p_{li}^c \rangle]}{\epsilon_{jl}^3(2\epsilon_{jl} - \epsilon_{ji}^3)} \delta(\epsilon_{jl} - \omega) + \frac{16Im[p_{ij}^a \langle p_{jl}^b p_{li}^c \rangle]}{\epsilon_{ji}^3(2\epsilon_{jl} - \epsilon_{ji})} \delta(\epsilon_{ji} - 2\omega) \right\}. \end{aligned} \quad (3)$$

Here $\epsilon_{ji} = \epsilon_{\mathbf{k}j} - \epsilon_{\mathbf{k}i}$ and $\langle p_{jl}^b p_{li}^c \rangle = \frac{1}{2}(p_{jl}^b p_{li}^c + p_{li}^b p_{jl}^c)$. The dipole transition matrix elements $p_{ij}^a = \langle \mathbf{k}j | \hat{p}_a | \mathbf{k}i \rangle$ were obtained from the self-consistent band structures within the PAW formalism²⁶. The real part of the second-order optical susceptibility is then obtained from $\chi_{abc}^{(2)}$ by a Kramer-Kronig transformation

$$\chi'^{(2)}(-2\omega, \omega, \omega) = \frac{2}{\pi} \mathbf{P} \int_0^\infty d\omega' \frac{\omega' \chi''^{(2)}(2\omega', \omega', \omega')}{\omega'^2 - \omega^2}. \quad (4)$$

The linear electro-optic coefficient $r_{abc}(\omega)$ is connected to the second-order optical susceptibility $\chi_{abc}^{(2)}(-\omega, \omega, 0)$ through the relation²⁷

$$\chi_{abc}^{(2)}(-\omega, \omega, 0) = -\frac{1}{2} n_a^2(\omega) n_b^2(\omega) r_{abc}(\omega) \quad (5)$$

where $n(\omega)$ is the refraction index in the a -direction. In the zero frequency limit,

$$\lim_{\omega \rightarrow 0} \chi_{abc}^{(2)}(-2\omega, \omega, \omega) = \lim_{\omega \rightarrow 0} \chi_{abc}^{(2)}(-\omega, \omega, 0). \quad (6)$$

Therefore,

$$r_{abc}(0) = -\frac{2}{n_a^2(0) n_b^2(0)} \lim_{\omega \rightarrow 0} \chi_{abc}^{(2)}(-2\omega, \omega, \omega). \quad (7)$$

Furthermore, for the photon energy $\hbar\omega$ well below the band gap, the linear electro-optic coefficient $r_{abc}(\omega) \approx r_{abc}(0)$ because $\chi_{abc}^{(2)}(-2\omega, \omega, \omega)$ and $n(\omega)$ are nearly constant in this low frequency region, as shown in the next Sec. and in Ref.²⁰.

In the present calculations, the δ -function in Eqs. 2-3 is approximated by a Gaussian function with $\Gamma = 0.2$ eV. The same k -point grid as in the DOS calculation is used. Furthermore, to ensure that ϵ' calculated via Kramer-Kronig transformation (Equ. 4) is reliable, at least ten energy bands per atom are included in the present optical calculations. The unit cell volume Ω in Eqs. 2-3 is not well defined for nanotubes. Therefore, like the previous calculations^{4,5,20}, we used the effective unit cell volume of the nanotubes rather than the volume of the supercells which is arbitrary. The effective unit cell of a nanotube is given by $\Omega = \pi[(D/2 + d/2)^2 - (D/2 - d/2)^2]T = \pi D d T$ where d is the thickness of the nanotube cylinder which is set to the interlayer distance of h -BN (3.28 Å²⁰). D and T are the diameter and length of translational vector of the nanotube²⁰, respectively.

III. RESULTS AND DISCUSSION

A. Hexagonal BN and single BN sheet

For comparison with the BN-NTs, we first investigated the second-order nonlinear optical susceptibility of both *h*-BN and an isolated honeycomb BN sheet. The isolated BN sheet is simulated by a slab-supercell approach with an inter-sheet distance of 6.5 Å. The theoretically determined lattice constants ($a = 2.486$ Å and $c = 6.562$ Å for *h*-BN and $a = 2.485$ Å for the BN sheet)²⁰ were used. Note that the theoretical lattice constants of *h*-BN agree rather well (within 1.5 %) with the experimental values ($a = 2.50$ Å and $c = 6.65$ Å)²⁸. Interestingly, we find numerically that although *h*-BN has zero second-order nonlinear optical susceptibility, the $\chi_{aab}^{(2)}$, $\chi_{baa}^{(2)}$ and $\chi_{bbb}^{(2)}$ for the isolated BN sheet are nonzero. Here a and b denote the two Cartesian coordinates within the BN layer. Moreover, $\chi_{baa}^{(2)} = \chi_{aab}^{(2)}$ and $\chi_{bbb}^{(2)} = -\chi_{aab}^{(2)}$. This is consistent with the symmetry consideration, demonstrating that our numerical method and calculations are qualitatively correct. Bulk *h*-BN should have zero second-order nonlinear optical susceptibility due to its spatial inversion symmetry. On the other hand, the isolated BN sheet does not have the spatial inversion symmetry (D_{6h}^4) and its symmetry class is D_{3h} ($P\bar{6}m2$). Therefore, the isolated BN sheet has nonzero $\chi_{aab}^{(2)}$, $\chi_{baa}^{(2)}$ and $\chi_{bbb}^{(2)}$ from the symmetry consideration.²⁹

In Fig. 1, the calculated real and imaginary parts as well as the absolute value of the imaginary part of $\chi_{aab}^{(2)}(-2\omega, \omega, \omega)$ of the single BN sheet are shown. In the calculations, a k -point grid of $100 \times 100 \times 2$ for the honeycomb BN sheet is used. It is clear from Fig. 1 that the second harmonic generation (SHG) coefficient $\chi_{aab}^{(2)}(-2\omega, \omega, \omega)$ is significant in the entire range of the optical photon energy ($\hbar\omega$). Furthermore, for the photon energy smaller than 2.2 eV, the $\chi_{aab}^{(2)}$ is purely dispersive (i.e., real and lossless) (Fig. 1a), suggesting that the BN sheet has potential application in nonlinear optical devices. Note that since the BN sheet has a theoretical band gap (E_g) of ~ 4.5 eV, the absorptive (imaginary) part of the $\chi_{aab}^{(2)}$ becomes nonzero only above the half of the band gap (i.e., ~ 2.2 eV). The real part of the $\chi_{aab}^{(2)}$ remains nearly constant at low photon energies up to 1.0 eV, then increases steadily in magnitude as the photon energy increases, and finally peaks at the absorption edge of ~ 2.2 eV (Fig. 1a). In the energy range from 2.5 to 5.5 eV, the real part of the $\chi_{aab}^{(2)}$ becomes positive and forms a broad double peak structure. Beyond 5.5 eV, it becomes negative again

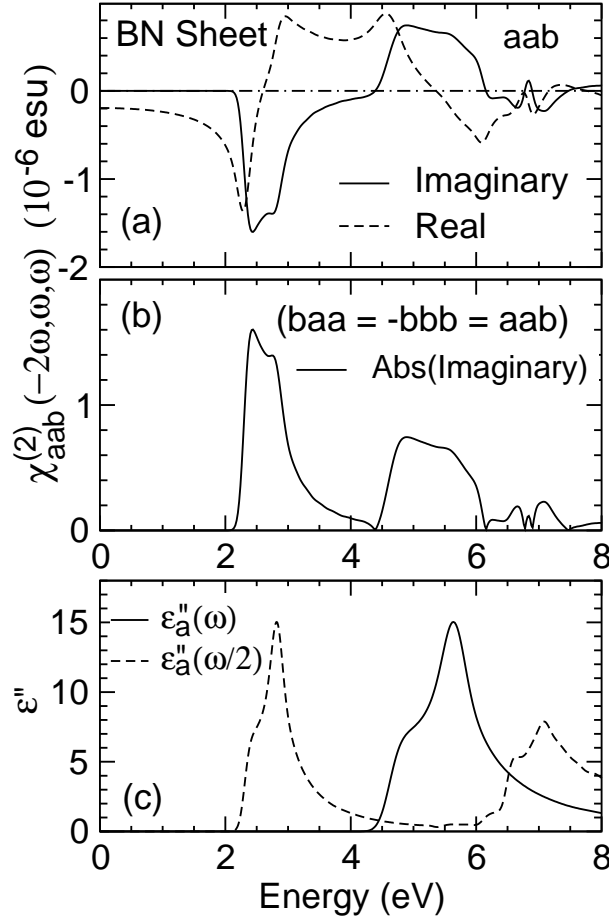


FIG. 1: (a) Real and imaginary parts as well as (b) the absolute value of the imaginary part of $\chi_{aab}^{(2)}(-2\omega, \omega, \omega)$ of the isolated BN sheet. In (c), $\varepsilon_a''(\omega)$ and $\varepsilon_a''(\omega/2)$ (imaginary part of the dielectric function) from Ref. ²⁰ are plotted.

and its magnitude gradually diminishes as the photon energy further increases (Fig. 1a).

The absorptive part of the $\chi_{aab}^{(2)}$ is nonzero only above ~ 2.2 eV, and looks like a Lorentzian oscillation between 2.2 and 6.0 eV with one sharp negative peak at ~ 2.5 eV and one broad positive peak around 5.5 eV (Fig. 1a). It is clear from Eqs. 2-3 that the calculated $\chi_{aab}^{(2)}$ spectra can have pronounced features due to both single- and double-frequency resonant terms. To analyze the features in the calculated $\chi^{(2)}$ spectra, it is helpful to compare the absolute value of $\chi''^{(2)}$ (Fig 1b) with the absorptive part of the corresponding dielectric function ε'' .³⁰ Therefore, the calculated ε'' from our previous publication²⁰ are shown in Fig. 1c as a function of both $\omega/2$ and ω . Clearly, the first sharp peak at ~ 2.5 eV is due

TABLE I: Calculated static refraction index n , second-order optical susceptibility $\chi^{(2)}(0)$ and linear electro-optical coefficient r_{abc} of the isolated BN sheet.

n_a (n_c)	$\chi_{bbb}^{(2)}, \chi_{aab}^{(2)}$ (pm/V)	r_{bbb}, r_{aab} (pm/V)
2.19 (1.63)	81.3, -81.3	-3.56, 3.56

to two-photon resonances [cf. $\varepsilon_a''(\omega/2)$] whilst in contrast, the second broad peak around 5.5 eV comes from the single-photon resonances [cf. $\varepsilon_a''(\omega)$]. Nevertheless, both single- and double-photon resonances involve only interband $\pi \rightarrow \pi^*$ and $\sigma \rightarrow \sigma^*$ optical transitions for the electric field vector \mathbf{E} polarized parallel to the BN layer ($E \parallel \hat{a}$)²⁰.

In Table I, the calculated zero frequency linear electro-optic coefficient $r(0)$ as well as the corresponding second-order nonlinear optical susceptibility $\chi^{(2)}(0,0,0)$ and the static refraction index $n(0)$ are listed. The refraction index $n(0)(= \sqrt{\varepsilon(0)})$ is derived from the calculated static dielectric constant $\varepsilon(0)$ which has been reported in our recent publication²⁰. Note that the $r(0)$ and $\chi^{(2)}(0,0,0)$ are listed in the SI pm/V unit, and 1 pm/V = 4.1888×10^{-8} esu. Significantly, the static second-order optical susceptibility for the isolated BN sheet is nearly thirty times larger than that of BN in both the zinc-blende and wurtzite structures³¹.

B. Second-order optical susceptibility

We have explicitly calculated the second-order optical susceptibility for the zigzag (5,0), (6,0), (8,0), (9,0), (12,0), (13,0), (15,0), (16,0), (17,0), (20,0), (21,0), (24,0), (25,0), (27,0), armchair (3,3), (4,4), (5,5), (6,6), (8,8), (12,12), (15,15), and chiral (4,2), (6,4), (8,4), (10,5) BN-NTs. In the calculations, a uniform grid ($1 \times 1 \times m$) along the tube axis (z-axis) was used. The number m is 200, 120, 150, 60, 100, 100, 80, 120, 80, 80, 60, 80, 60, 60 for the zigzag BN-NTs, respectively, and 60, 50, 40, 60 for the chiral BN-NTs, respectively. In the case of CNTs, only the chiral nanotubes would exhibit second-order nonlinear optical behavior with two nonvanishing components of xyz and xzy of $\chi^{(2)}$.⁴ Here z refers to the coordinate along the tube axis whilst x and y denote the two coordinates that are perpendicular to the tube axis. As for CNTs, the armchair BN-NTs are found not to have any nonzero components of $\chi^{(2)}$. In contrast, both the zigzag and chiral BN-NTs are found to show second-order nonlinear optical behavior. Specifically, all the zigzag BN-NTs except (5,0),

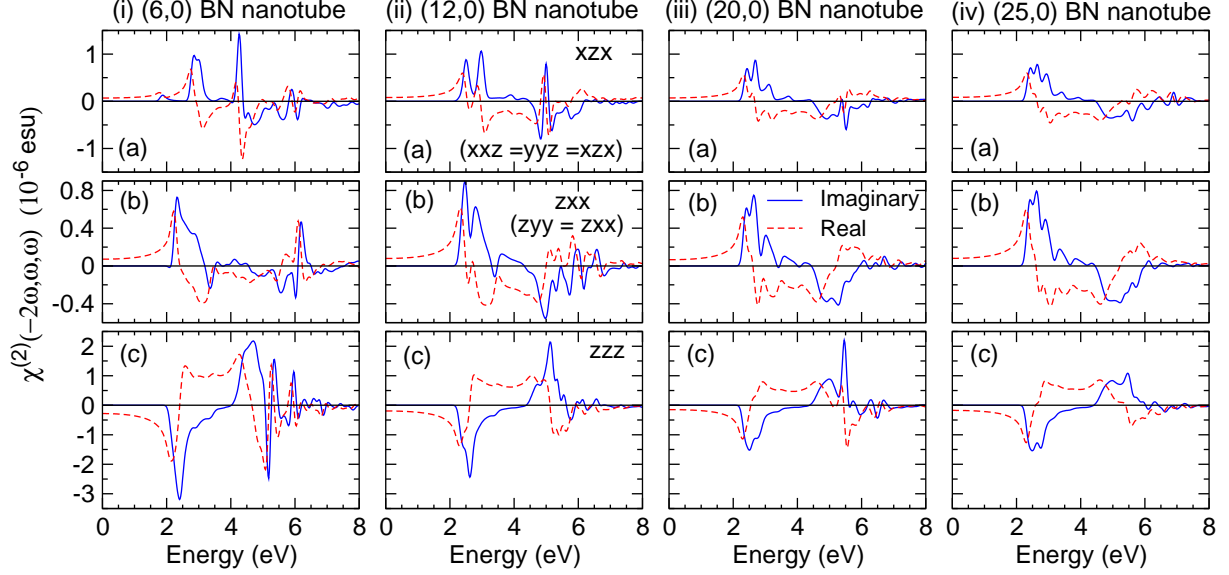


FIG. 2: (Color online) Real and imaginary parts of $\chi^{(2)}(-2\omega, \omega, \omega)$ of the zigzag (6,0), (12,0), (20,0) and (25,0) BN nanotubes.

(9,0) and (27,0), have six nonvanishing components of the second-order optical susceptibility, namely, xzx , xxz , yyz , zxx , zyy , zzz . Nevertheless, these components are not completely independent of each other. In particular, $\chi_{xxz}^{(2)} = \chi_{yyz}^{(2)} = \chi_{xzx}^{(2)}$, and $\chi_{zyy}^{(2)} = \chi_{zxx}^{(2)}$. This finding is especially important for the application of BN-NTs in nonlinear optical devices because most BN-NTs tend to have a zigzag structure,⁹ as mentioned before. The chiral BN-NTs have eight nonvanishing components of the second-order optical susceptibility with two additional nonzero components being xyz and yzx . Note that $\chi_{yzx}^{(2)} = -\chi_{xyz}^{(2)}$. These numerical findings are consistent with the consideration of the symmetry of the BN nanotubes. The point symmetry groups of the BN-NTs¹¹ are C_{2nv} for zigzag $(n,0)$ nanotubes, C_{2nh} for armchair (n,n) nanotubes, and C_N for chiral (n,m) nanotubes where $N = 2(n^2 + m^2 + nm)/d_R$ with d_R being the greatest common divisor of $2n + m$ and $2m + n$. Therefore, these symmetries would dictate²⁹ that all the components vanish for armchair (n,n) nanotubes, and that nonvanishing components for zigzag $(n,0)$ nanotubes are $xzx = yzy$, $xxz = yyz$, $zxx = zyy$, zzz , as well as that nonvanishing components of chiral (n,m) nanotubes include all that for zigzag $(n,0)$ nanotubes plus $xyz = -yzx$. We don't know at the moment why the (5,0), (9,0) and (27,0) BN-NTs are found numerically to have no nonzero components though they don't have to from their symmetry point of view.

In Fig. 2, the calculated real and imaginary parts of the second-order optical suscep-

tibility $\chi^{(2)}(-2\omega, \omega, \omega)$ for the four selected zigzag nanotubes [(6,0), (12,0), (20,0), and (25,0)] are shown. As for the single BN sheet, the second harmonic generation coefficients $\chi^{(2)}(-2\omega, \omega, \omega)$ for the zigzag BN-NTs are significant in the entire range of the optical photon energy ($\hbar\omega$). Indeed, they are generally more than ten times larger than that of bulk BN in the zinc-blende and wurtzite structures.³¹ Moreover, for the photon energy smaller than 2.0 eV, the $\chi^{(2)}$ is purely dispersive (i.e., real and lossless) (Fig. 2). Interestingly, the magnitude of $\chi_{zzz}^{(2)}$ is the largest and in general about three times larger than that of the other nonvanishing components (Fig. 2). For $\chi_{zzz}^{(2)}$, the electric field of both the incoming and outgoing photons is polarized parallel to the tube axis and thus the electric dipolarization effect would be essentially zero²⁰. This may be particularly important for nonlinear optical applications. We also note that the shape of the spectra of $\chi_{zzz}^{(2)}$ and $\chi_{zxx}^{(2)}$ for all the zigzag BN-NTs look very similar, except the difference in sign. For the zigzag BN-NTs with a larger diameter such as (12,0), (20,0) and (25,0), the spectrum of $\chi_{xzx}^{(2)}$ is also similar to that of $\chi_{zxx}^{(2)}$ (Fig. 2). The magnitude of all the components decreases somewhat as the diameter of the tubes increases [e.g., from (6,0) to (12,0)], but however, becomes stable as the diameter further increases [see, e.g., (20,0) and (25,0) in Fig. 2]. Furthermore, both the magnitude and shape of the $\chi_{zzz}^{(2)}$ spectrum for the zigzag BN-NTs with a larger diameter, e.g., (25,0), approach to that of the single BN sheet (Fig. 1 and Fig. 2), as they should.

As for the single BN sheet, in order to understand the features in the calculated $\chi^{(2)}$ spectra of the zigzag BN-NTs, the absolute values of the imaginary part $\chi''^{(2)}$ of all the nonzero components of the (12,0) BN-NT are plotted and compared with the absorptive part of the dielectric function ε'' from our previous publication²⁰ in Fig. 3. Strikingly, the first prominent peak between 2.0 and 4.0 eV in the $\chi_{zzz}''^{(2)}$ spectrum is almost identical to the first peak in the $\varepsilon_z''(\omega/2)$ (see Fig. 3d-e), indicating that it is due to two-photon resonances. In contrast, the second peak between 4.5 and 5.5 eV in the $\chi_{zzz}''^{(2)}$ spectrum is very similar to the first peak in the $\varepsilon_z''(\omega)$, suggesting that it is caused by the single-photon resonances. Nevertheless, both these single- and double-photon resonances involve only interband $\pi \rightarrow \pi^*$ and $\sigma \rightarrow \sigma^*$ optical transitions for the electric field vector \mathbf{E} polarized parallel to the tube axis ($E \parallel \hat{z}$)²⁰. Fig. 3 also shows that the double-peak structure between 2.0 and 4.0 eV in both the $\chi_{xzz}''^{(2)}$ and $\chi_{zxx}''^{(2)}$ spectra is mainly due to the two-photon resonances with $E \perp \hat{z}$ [cf. $\varepsilon_x''(\omega/2)$] (see Fig. 3a-c), while, in contrast, the second feature in the photon energies above 4.5 eV perhaps comes predominantly from the single-photon resonances for $E \perp \hat{z}$.

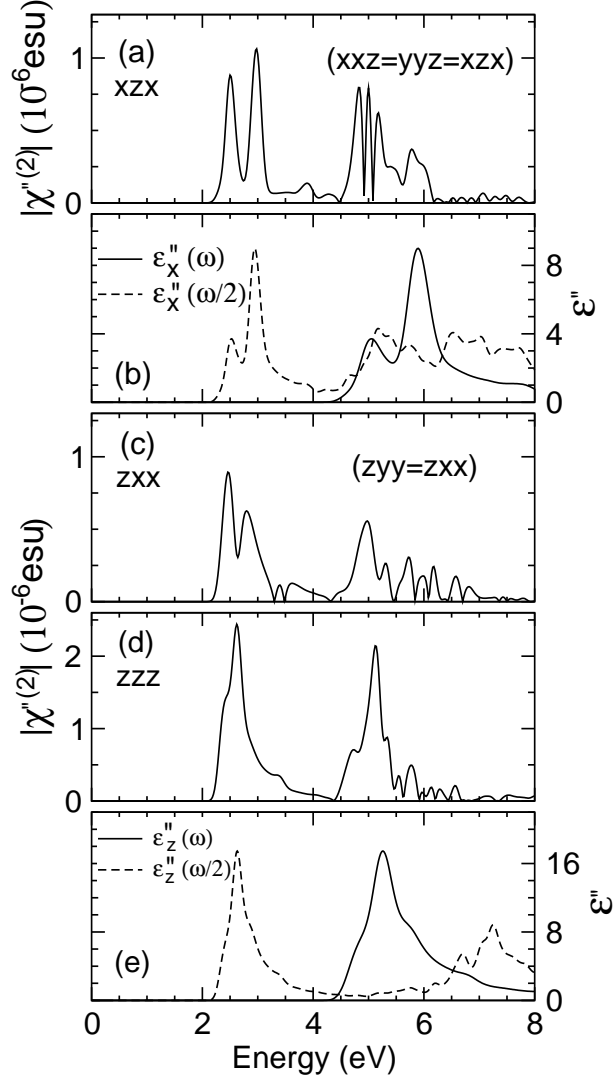


FIG. 3: Absolute value of the imaginary part of $\chi^{(2)}(-2\omega, \omega, \omega)$ (a, c, d) as well as $\varepsilon''_a(\omega)$ and $\varepsilon''_a(\omega/2)$ (imaginary part of the dielectric function) (b, e) from Ref. ²⁰ of the zigzag (12,0) BN nanotube.

[cf. $\varepsilon''_x(\omega)$]. This conclusion is further supported by the fact that the magnitude of $\varepsilon''_x(\omega)$ ($\varepsilon''_x(\omega/2)$) is only about half of that of $\varepsilon''_z(\omega)$ ($\varepsilon''_z(\omega/2)$), and concurrently the magnitude of $\chi''_{xxz}^{(2)}$ and $\chi''_{zxx}^{(2)}$ is only about half of that of $\chi''_{zzz}^{(2)}$ too.

In Fig. 4, the calculated real and imaginary parts of the second-order optical susceptibility $\chi^{(2)}(-2\omega, \omega, \omega)$ for all the four chiral nanotubes [(4,2), (6,2), (8,4) and (10,5)] are displayed. In general, the spectra of each component of the second-order optical susceptibility for all the chiral BN-NTs are similar, except that the magnitude decreases somewhat as the diameter of the tubes increases. The decrease of the magnitude with the tube diameter is particularly

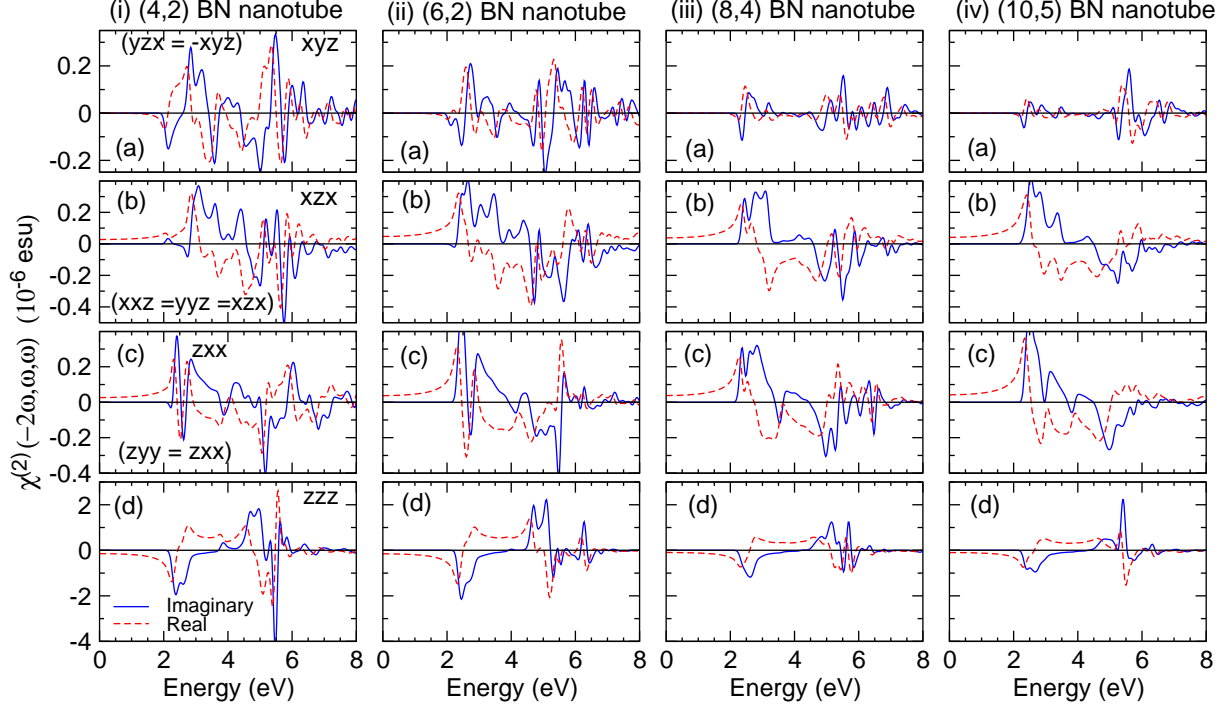


FIG. 4: (Color online) Real and imaginary parts of $\chi^{(2)}(-2\omega, \omega, \omega)$ of the chiral (4,2), (6,2), (8,4) and (10,5) BN nanotubes.

apparent for the xyz and zzz components. For all the chiral BN-NTs, remarkably, the zzz component is nearly ten times larger than all the other nonvanishing components. Another common feature is that both the real and imaginary parts of $\chi^{(2)}(-2\omega, \omega, \omega)$ show a rather oscillatory behavior, particularly for the xyz and xzx components (Fig. 4). The amplitude of these oscillatory real and imaginary parts is rather large in the photon energies of 2.0~6.0 eV for the chiral BN-NTs with a small diameter. It should also be noted that the shape and magnitude of the xzx and zxx components look very much alike (Fig. 4b-c).

Again, in order to understand the structures in the calculated $\chi^{(2)}$ spectra of the chiral BN-NTs, the absolute values of the imaginary part $\chi''^{(2)}$ of all the nonzero components of the (6,2) BN-NT are plotted and compared with the absorptive part of the corresponding dielectric function ε'' from our previous publication²⁰ in Fig. 5. Remarkably, the first prominent peak between 2.0 and 4.0 eV in the $\chi_{zzz}''^{(2)}$ spectrum is almost identical to the first peak in the $\varepsilon_z''(\omega/2)$ (see Fig. 5d-e), indicating that it is due to two-photon resonances. On the other hand, the second structure between 4.5 and 5.5 eV in the $\chi_{zzz}''^{(2)}$ spectrum may be correlated with the first peak in the $\varepsilon_z''(\omega)$, suggesting that it is caused by the single-

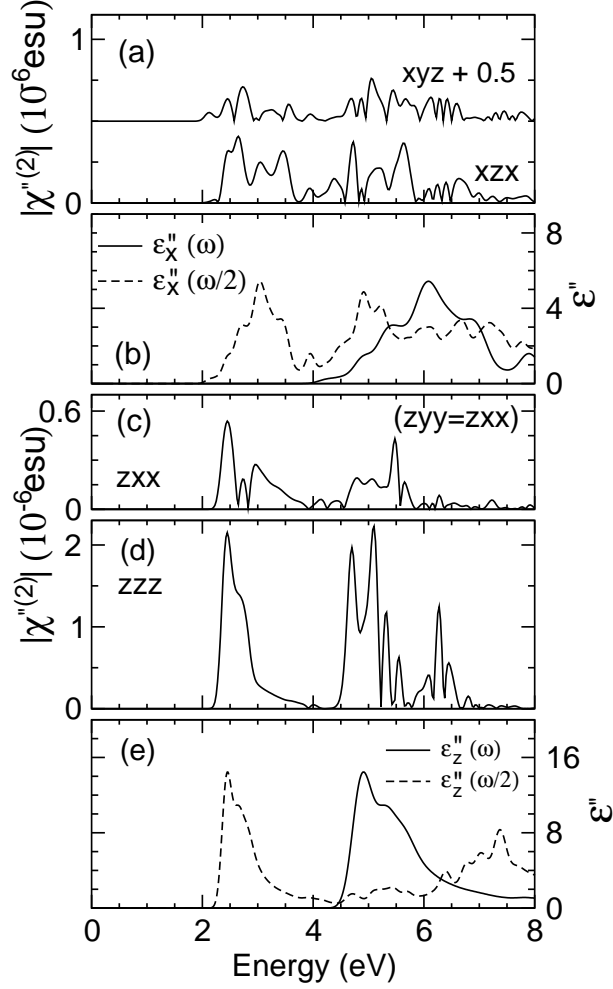


FIG. 5: Absolute value of the imaginary part of $\chi^{(2)}(-2\omega, \omega, \omega)$ (a, c, d) and $\varepsilon''_a(\omega)$ and $\varepsilon''_a(\omega/2)$ (imaginary part of the dielectric function) (b, e) from Ref. ²⁰ of the zigzag (6,2) BN nanotube.

photon resonances. As for the zigzag BN-NTs, both these single-photon and double-photon resonances involve only interband $\pi \rightarrow \pi^*$ and $\sigma \rightarrow \sigma^*$ optical transitions for the electric field vector \mathbf{E} polarized parallel to the tube axis ($E \parallel \hat{z}$)²⁰. Fig. 5 further suggests that the feature between 2.0 and 4.0 eV in the spectra of both the $\chi''^{(2)}_{xzx}$ and $\chi''^{(2)}_{zxx}$ as well as $\chi''^{(2)}_{xyz}$ may be attributed to the two-photon resonances with $E \perp \hat{z}$ [cf. $\varepsilon''_x(\omega/2)$] (see Fig. 5a-c), while, in contrast, the second feature in the photon energies above 4.5 eV is mainly due to the single-photon resonances for $E \perp \hat{z}$ [cf. $\varepsilon''_x(\omega)$]. One exception is that the narrow peak at 2.5 eV in the $\chi''^{(2)}_{zxx}$ spectrum (Fig. 5c) which may come predominantly from the two-photon resonances with $E \parallel \hat{z}$ [cf. $\varepsilon''_z(\omega/2)$ in Fig. 5e].

TABLE II: Calculated static refraction index n , second-order optical susceptibility $\chi^{(2)}$ and linear electro-optical coefficient r_{abc} of the zigzag and chiral BN nanotubes.

	n_x (n_z)	$\chi_{xx}^{(2)}, \chi_{zx}^{(2)}, \chi_{zz}^{(2)}$ (pm/V)	r_{xx}, r_{zx}, r_{zz} (pm/V)
(5,0)	1.88 (2.22)	0.0, 0.0, 0.0	0.0, -0.0, 0.0
(6,0)	1.89 (2.21)	29.1, 33.2, -117.9	-3.34, -3.81, 9.88
(8,0)	1.90 (2.20)	32.1, 32.3, -97.6	-3.67, -3.70, 8.33
(9,0)	1.89 (2.17)	0.0, 0.0, 0.0	0.0, 0.0, 0.0
(12,0)	1.89 (2.17)	33.5, 33.2, -81.2	-3.98, -3.95, 7.32
(13,0)	1.91 (2.18)	35.3, 35.1, -83.0	-4.07, -4.05, 7.35
(15,0)	1.89 (2.17)	34.9, 34.6, -78.8	-4.15, -4.11, 7.11
(16,0)	1.91 (2.18)	36.4, 36.5, -81.1	-4.20, -4.21, 7.18
(17,0)	1.91 (2.18)	36.1, 36.3, -79.8	-4.16, -4.19, 7.06
(20,0)	1.87 (2.16)	30.0, 27.7, -61.8	-3.68, -3.40, 5.58
(21,0)	1.90 (2.18)	35.7, 35.8, -76.5	-4.16, -4.17, 6.77
(24,0)	1.90 (2.18)	35.8, 35.6, -75.2	-4.17, -4.15, 6.66
(25,0)	1.90 (2.17)	33.7, 33.8, -73.0	-3.96, -3.98, 6.58
(27,0)	1.89 (2.16)	0.0, 0.0, 0.0	0.0, 0.0, 0.0
(12,0)@(20,0)	1.95 (2.20)	10.1, 10.3, -19.3	-1.10, -1.12, 1.65
(12,0) bundle	1.92 (2.19)	37.0, 38.3, -89.0	-4.19, -4.33, 7.74
(4,2)	1.92 (2.14)	11.5, 11.5, -61.8	-1.36, -1.36, 5.89
(6,2)	1.89 (2.15)	15.8, 15.8, -64.9	-1.91, -1.91, 6.07
(8,4)	1.89 (2.15)	16.0, 16.0, -40.6	-1.94, -1.94, 3.80
(10,5)	1.89 (2.15)	17.5, 17.5, -41.3	-2.12, -2.12, 3.87

C. Linear electro-optical coefficient

In Table II, the calculated zero frequency linear electro-optic coefficient $r(0)$ as well as the corresponding second-order nonlinear optical susceptibility $\chi^{(2)}(0,0,0)$ are listed. The $r(0)$ is calculated from the corresponding $\chi^{(2)}(0,0,0)$ by using Equ. 7. The refraction index $n(0)(= \sqrt{\varepsilon(0)})$ is derived from the calculated static dielectric constant $\varepsilon(0)$ which

has been reported in our recent publication²⁰. Table II shows that apart from the (5,0), (9,0) and (27,0) BN-NTs which have no nonvanishing $r_{abc}(0)$, all the other zigzag BN-NTs have very similar linear electro-optical coefficients, as for the static dielectric constant and polarizability²⁰. Nevertheless, $r_{zzz}(0)$ decreases slightly as the diameter increases, while $r_{xzx}(0)$ and $r_{zxx}(0)$ increase slightly as the diameter goes up. We note that $\chi_{xzx}^{(2)}$ and $\chi_{zxx}^{(2)}$ are virtually identical, while $\chi_{zzz}^{(2)}$ is about two times larger than $\chi_{xzx}^{(2)}$ and $\chi_{zxx}^{(2)}$.

The chiral BN-NTs have two additional nonvanishing components $\chi_{xyz}^{(2)}$ and $\chi_{yzx}^{(2)}$. Nevertheless, the calculated static values of $\chi_{xyz}^{(2)}$ and $\chi_{yzx}^{(2)}$ are zero, satisfying the requirement by the so-called Kleinman symmetry³² which demands that $\chi_{xyz}^{(2)}(0) = \chi_{yzx}^{(2)}(0)$. Consequently, the corresponding static linear electro-optical coefficients $r_{xyz}(0)$ and $r_{yzx}(0)$ are zero too. Therefore, $\chi_{yzx}^{(2)}$, $\chi_{xyz}^{(2)}$, $r_{xyz}(0)$ and $r_{yzx}(0)$ for the chiral BN-NTs are not listed in Table II. As for the nonvanishing static components, $r_{xzx}(0)$ and $r_{zxx}(0)$ for the (6,2), (8,4) and (10,5) BN-NTs are rather close, while $r_{zzz}(0)$ for the (6,2) BN-NT is nearly 1.6 times larger than that for the (8,4) and (10,5) BN-NTs. Though $r_{zzz}(0)$ for the (4,2) BN-NT is close to that of the (6,2) BN-NT, $r_{xzx}(0)$ and $r_{zxx}(0)$ for the (4,2) is somewhat smaller than that of the other armchair BN-NTs.

Group III nitrides are promising materials for nonlinear optical and opto-electric applications because of their unique physical properties such as a wide band gap. However, the static $\chi^{(2)}(0)$ and hence $r(0)$ of bulk BN structures are the smallest among the group III nitrides (see, e.g.,³¹). It is therefore remarkable that BN in the single-walled zigzag BN-NTs and their bundles has greatly enhanced static second-order nonlinear optical susceptibility and linear electro-optical coefficient. This enhancement can be as large as thirty folds (see Table II and Ref.³¹), and it could make the BN nanotube structures have the largest $\chi^{(2)}$ and r among the nitrides. In fact, the static $\chi^{(2)}(0)$ of the zigzag BN-NTs is up to five times larger than that of GaN which has the largest $\chi^{(2)}(0)$ among the bulk group III nitrides.³¹

D. Effects of interwall interactions

We have so far focused only on the nonlinear optical properties of single-walled BN-NTs. However, BN-NTs are usually multiwalled or in the format of bundles. Therefore, to study the possible effects of interwall interactions on the nonlinear optical properties of BN-NTs, we have also considered a double-walled BN-NT, namely, the zigzag (12,0)@(20,0), and a

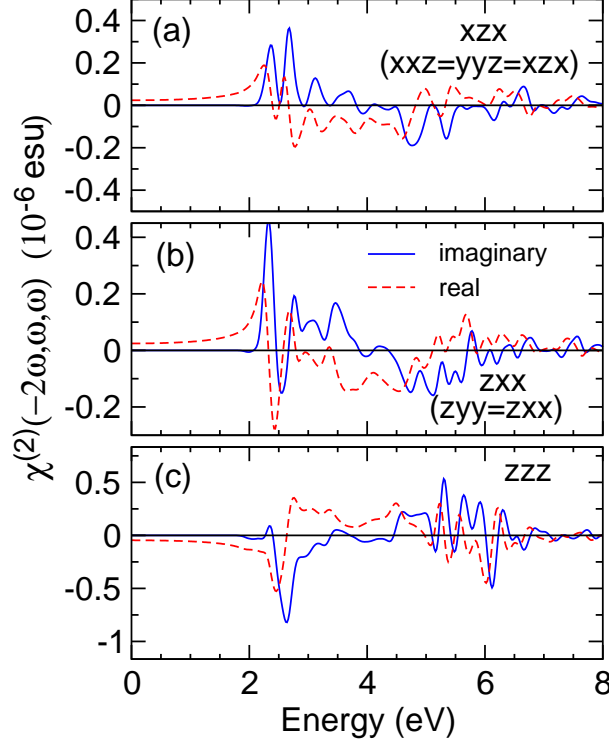


FIG. 6: (Color online) Real and imaginary parts of $\chi^{(2)}(-2\omega, \omega, \omega)$ of the double-walled (12,0)@(20,0) BN nanotube.

single-walled zigzag (12,0) BN-NT bundle. The double-walled nanotube is chosen because BN-NTs typically have a zigzag structure, and also the interwall distance of about 3.2 Å between the (12,0) and (20,0) nanotubes is close to the interlayer distance in *h*-BN. The BN-NT bundle was modelled by a two-dimensional hexagonal array with the initial interwall distance between adjacent nanotubes being about 3.2 Å. The atomic positions and lattice constants were then fully relaxed by a conjugate gradient technique. Theoretical equilibrium nanotube structures were obtained when the forces acting on all the atoms and the uniaxial stress were less than 0.03 eV/Å and 2.0 kBar, respectively. The theoretical determined atomic structures were used in the electronic structure and optical property calculations. The calculated density of states and dielectric function of the (12,0)@(20,0) double-walled BN-NT have already been reported in Ref. ²⁰.

The calculated second-order optical susceptibility of the double-walled (12,0)@(20,0) BN-NT is shown in Fig. 6. A uniform grid of $1 \times 1 \times 60$ in the Brillouin zone was used. Figs. 2 and 6 show that broadly speaking, each component of the second-order optical susceptibility of the (12,0)@(20,0) BN-NT is rather similar to the corresponding component of the (12,0)

and (20,0) BN-NTs. However, the magnitude of the second-order optical susceptibility of the double-walled BN-NT is significantly reduced in comparison with that of the (12,0) and (20,0) BN-NTs. In particular, the magnitude of the zzz component of the (12,0)@(20,0) BN-NT is about three and two times smaller than that of the (12,0) and (20,0) BN-NTs, respectively (Figs. 2 and 6). In contrast, the density of states and dielectric function of the (12,0)@(20,0) as well as (12,0) and (20,0) BN-NTs are very similar,²⁰ indicating that the effects of interwall interaction on the electronic structure and linear optical properties would be small. In particular, the dielectric function of the (12,0)@(20,0) is nearly the same as that of the (20,0). The reduction in the magnitude of $\chi^{(2)}$ may be explained by the fact that bulk h -BN does not show second-order nonlinear optical behavior and that a multi-walled BN-NT with a very large diameter is essentially equivalent to h -BN. Another discernable difference is that the second-order optical susceptibility of the (12,0)@(20,0) BN-NT is considerably more oscillatory than that of the (12,0) and (20,0) BN-NTs.

The static SHG and linear electro-optic coefficients are compared with the single-walled BN-NTs in Table II. Although the static refraction index of the (12,0)@(20,0) BN-NT is almost identical to that of the single-walled BN-NTs, the static SHG coefficient is more than three times smaller than that of the single-walled zigzag nanotubes. Consequently, the linear electro-optical coefficient of the double-walled nanotube is several times smaller than that of the single-walled zigzag nanotubes (Table II).

The calculated second-order optical susceptibility of the (12,0) BN-NT bundle is shown in Fig. 7. A uniform grid of $6 \times 6 \times 60$ in the Brillouin zone was used. The effective unit cell volume is used in order to compare quantitatively the optical properties of the bundle with that of the isolated (12,0) BN nanotube. Nevertheless, the use of the solid unit cell volume of the bundle would only uniformly reduce the amplitude of the calculated second-order optical susceptibility by a factor of 1.43 but would not change its shape. Figs. 2 and 7 show that each component of the second-order optical susceptibility of the (12,0) BN-NT bundle is similar to the corresponding component of the isolated single-walled (12,0) BN-NT in both the shape and magnitude. In particular, the zzz component of the (12,0) BN-NT bundle is nearly identical to that of the isolated (12,0) BN-NT (Figs. 2 and 7). This clearly shows that the interwall interaction between the BN-NTs in the bundle has essentially no effect on the second-order nonlinear optical properties, in strong contrast to the case of the multi-walled BN-NTs. We also find that the dielectric function of the (12,0) BN-NT bundle

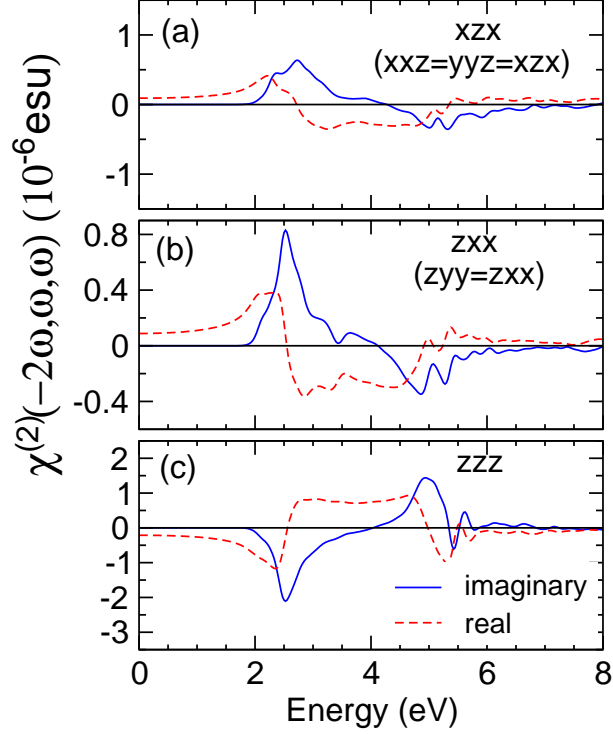


FIG. 7: (Color online) Real and imaginary parts of $\chi^{(2)}(-2\omega, \omega, \omega)$ of the single-walled (12,0) BN-NT bundle.

(not shown here) is nearly the same as that of the isolated single-walled (20,0) BN-NT. Nevertheless, there are minor differences in the second-order optical susceptibility between the isolated (12,0) BN-NT and the (12,0) BN-NT bundle. For example, the second-order optical susceptibility of the isolated (12,0) BN-NT is somewhat more oscillatory than that of the (12,0) BN-NT bundle. This minor difference might be due to the fact that more k -points for the (12,0) BN-NT bundle were used than for the single (12,0) BN-NT.

The static SHG and linear electro-optic coefficients are compared with the single-walled BN-NTs in Table II. Unlike the case of the double walled BN-NT, the static SHG linear and electro-optic coefficients of the single-walled (12,0) BN-NT bundle are rather similar to that of the single-walled BN-NTs (Table II). This clearly shows that the interwall interaction hardly has any effect on the nonlinear optical properties, in strong contrast to the double walled BN-NT where the interwall interaction significantly reduce the SHG and linear electro-optic coefficients. Indeed, the SHG and linear electro-optic coefficients of the (12,0) BN-NT bundle are slightly enhanced, as compared with that of the single (12,0) BN-NT (Table II). This is rather significant because in the nonlinear optical applications,

one would usually need the BN-NTs in the format of either multiwalled BN-NTs or BN-NT bundles. The present work therefore suggests that the single-walled BN-NT bundles would be preferred for nonlinear optical and electro-optical applications.

IV. SUMMARY

We have carried out a systematic *ab initio* study of the second-order nonlinear optical properties of the BN-NTs within density functional theory in the local density approximation. We used the highly accurate full-potential PAW method. The underlying atomic structure of the BN nanotubes was determined theoretically. Specifically, the properties of the single-walled zigzag [(5,0), (6,0), (8,0), (9,0), (12,0), (13,0), (15,0), (16,0), (17,0), (20,0), (24,0), (25,0), (27,0)], armchair [(3,3), (4,4), (5,5), (6,6), (8,8), (12,12), (15,15)], and chiral [(4,2), (6,2), (8,4), (10,5)] nanotubes as well as the double-walled (12,0)@(20,0) nanotube and the single-walled (12,0) nanotube bundle have been calculated. For comparison, the second-order nonlinear optical properties of *h*-BN and the single BN sheet have also been calculated. Interestingly, we find that though *h*-BN has zero second-order nonlinear optical susceptibility, the $\chi_{aab}^{(2)}$, $\chi_{baa}^{(2)}$ and $\chi_{bbb}^{(2)}$ for the isolated BN sheet are large and generally several ten times larger than that of bulk BN in both the zinc-blende and wurtzite structures. We also find that, unlike carbon nanotubes, both the chiral and zigzag BN-NTs have pronounced second-harmonic generation and linear electro-optical coefficients which are comparable to that of the single BN sheet. The prominent structures in the spectra of $\chi^{(2)}(-2\omega, \omega, \omega)$ of the BN-NTs have been successfully correlated with the features in the corresponding linear optical dielectric function $\varepsilon(\omega)$ in terms of single-photon and double-photon resonances. Though the interwall interaction in the double-walled BN-NTs is found to reduce the second-order nonlinear optical coefficients significantly, the interwall interaction in the single-walled BN-NT bundle has essentially no effect on the nonlinear optical properties, suggesting that the single-walled BN-NTs and single-walled BN-NT bundles are promising nonlinear optical materials for applications in, e.g., second-harmonic generation, sum frequency generation and electro-optical switches. We hope that this work would stimulate experimental investigations into the second-order nonlinear optical properties of BN-NTs.

V. ACKNOWLEDGMENTS

The authors thank Ding-Sheng Wang and Chung-Gang Duan for helpful discussions and for allowing to access their nonlinear optical calculation program. The authors gratefully acknowledge financial supports from National Science Council, Ministry of Economic Affairs (93-EC-17-A-08-S1-0006) and NCTS/TPE of the Republic of China. They also thank National Center for High-performance Computing of Taiwan for providing CPU time.

-
- ¹ S. Iijima, *Nature* (London) **354**, 56 (1991).
- ² M. Bockrath, D.H. Cobden, J. Lu, A.G. Rinzler, R.E. Smalley, L. Balents and P.L. McEuen, *Nature* (London) **397**, 598 (1999).
- ³ L. Liu, G.Y. Guo, C.S. Jayanthi and S.Y. Wu, *Phys. Rev. Lett.* **88**, 217206 (2002).
- ⁴ G.Y. Guo, K.C. Chu, D.-S. Wang, and C.-G. Duan, *Phys. Rev. B* **69**, 205416 (2004).
- ⁵ G.Y. Guo, K.C. Chu, D.-S. Wang, and C.-G. Duan, *Comp. Mater. Sci.* **30**, 269 (2004).
- ⁶ A. Rubio, J.L. Corkill and M.L. Cohen, *Phys. Rev. B* **49**, R5081 (1994)
- ⁷ X. Blase, A. Rubio, S.G. Louie, and M.L. Cohen, *Europhys. Lett.* **28**, 335 (1994)
- ⁸ e.g., N.G. Chopra, R.J. Luyken, K. Cherrey, V.H. Crespi, M.L. Cohen, S.G. Louie, and A. Zettl, *Science* **28**, 335 (1994); A. Loiseau, F. Willaime, N. Demoncy, G. Hug, and H. Pascard, *Phys. Rev. Lett.* **76**, 4737 (1996).
- ⁹ R.S. Lee, J. Gavillet, M. Lamy de la Chapelle, A. Loiseau, J.-L. Cochon, D. Pigache, J. Thibault, and F. Willaime, *Phys. Rev. B* **64**, 121405(R) (2001).
- ¹⁰ Y. Chen, J. Zou, S.J. Campbell, and G.L. Caer, *Appl. Phys. Lett.* **84**, 2430 (2004).
- ¹¹ O.E. Alon, *Phys. Rev. B* **64**, 153408 (2001).
- ¹² Y.-H. Kim, K.J. Chang and S.G. Louie, *Phys. Rev. B* **63**, 205408 (2001).
- ¹³ E.J. Mele and P. Kral, *Phys. Rev. Lett.* **88**, 56803 (2002). *Soc. Jpn.* **71**, 2286 (2002).
- ¹⁴ S. Okada, S. Saito, and A. Oshiyama, *Phys. Rev. B* **65**, 165410 (2002).
- ¹⁵ R.B. Chen, F.L. Shyu, C.P. Chang, and M.F. Lin, *J. Phys. Soc. Jpn.* **71**, 2286 (2002).
- ¹⁶ B. Akdim, R. Pachter, X. Duan, and W. Wade Adams, *Phys. Rev. B* **67**, 245404 (2003).
- ¹⁷ H.J. Xiang, J. Yang, J.G. Hou, and Q. Zhu, *Phys. Rev. B* **68**, 35427 (2003).

- ¹⁸ M.-F. Ng and R.Q. Zhang, Phys. Rev. B **69**, 115417 (2004).
- ¹⁹ A.G. Marinopoulos, L. Wirtz, A. Marini, V. Olevano, A. Rubio, and L. Reining, Appl. Phys. A **78**, 1157 (2004).
- ²⁰ G.Y. Guo, and J.C. Lin, Phys. Rev. B **71**, 165402 (2005).
- ²¹ T.S. Bartnitskaya, G.S. Oleinik, A.V. Pokropivnyi, and V.V. Pokropivnyi, JETP Lett. **69**, 163 (1999).
- ²² P.E. Blöchl, Phys. Rev. B **50**, 17953 (1994); G. Kresse and D. Joubert, Phys. Rev. B **59**, 1758 (1999).
- ²³ G. Kresse and J. Hafner, Phys. Rev. B **47**, R558 (1993); **49**, 14251 (1994); G. Kresse and J. Furthmüller, Comput. Mater. Sci. **6**, 15 (1996).
- ²⁴ C.-G. Duan, J. Li, Z.-Q. Gu, and D.-S. Wang, Phys. Rev. B **60**, 9435 (1999).
- ²⁵ Ed. Ghahramani, D.J. Moss and J.E. Sipe, Phys. Rev. Lett. **64**, 2815 (1990); *ibid*, Phys. Rev. B **43**, 8990 (1991).
- ²⁶ B. Adolph, J. Furthmüller, and F. Bechstedt, Phys. Rev. B **63**, 125108 (2001).
- ²⁷ J.L.P. Hughes and J.E. Sipe, Phys. Rev. B **53**, 10751 (1996).
- ²⁸ G. Cappellini, V. Fiorentini, K. Tenelsen, and F. Bechstedt, in *Gallium Nitride and Related Materials*, edited by R.D. Dupuis, J.A. Edmond, F.A. Ponce, and S. Nakamura, Mater. Res. Soc. Symp. Proc. No. **395** (Materials Research Society, Pittsburgh, 1996).
- ²⁹ R.W. Boyd, *Nonlinear Optics* (Elsevier, Amsterdam, 2003).
- ³⁰ J.E. Sipe, A.I. Shkrebtii, and O. Pulci, Phys. Status Solidi A **170**, 431 (1998).
- ³¹ V.I. Gavrilenko and R.Q. Wu, Phys. Rev. B **61**, 2632 (2000).
- ³² D.A. Kleinmam, Phys. Rev. **126**, 1977 (1962).